Gamow-Teller strength of ^{90}Nb in the continuum studied via multipole decomposition analysis of the ^{90}Zr(p,n) reaction at 295 MeV

T. Wakasa,* H. Sakai, H. Okamura, H. Otsu, S. Fujita,† S. Ishida,‡ N. Sakamoto,‡ T. Uesaka, and Y. Satou
Department of Physics, University of Tokyo, Bunkyo, Tokyo 113, Japan

M. B. Greenfield
International Christian University, Mitaka, Tokyo 181, Japan

K. Hatanaka
Research Center for Nuclear Physics, Osaka University, Ibaraki, Osaka 567, Japan
(Received 6 November 1996)

The double differential cross sections at $\theta_{\rm lab}$ between 0.0° and 12.3° and the polarization transfer D_{NN} at 0° for the ^{90}Zr(p,n) reaction are measured at a bombarding energy of 295 MeV. A multipole decomposition technique is applied to the cross sections to extract $L=0$, $L=1$, $L=2$, and $L=3$ contributions. The Gamow-Teller (GT) strength B(GT) in the continuum deduced from the $L=0$ cross section is compared both with the perturbative calculation by Bertsch and Hamamoto and with the second-order random phase approximation calculation by Drożdż *et al.* The sum of B(GT) values up to 50 MeV excitation becomes $S_{\beta^-}=28.0\pm1.6$ after subtracting the contribution of the isovector spin-monopole strength. This S_{β^-} value of 28.0 ± 1.6 corresponds to about (93 ± 5)% of the minimum value of the sum rule $3(N-Z)=30$. The usefulness of the polarization transfer observable in the distorted wave impulse approximation is presented. [S0556-2813(97)02006-2]

PACS number(s): 24.30.Cz, 25.40.Kv, 27.60.+j

I. INTRODUCTION

The nucleon-nucleus charge exchange reaction at intermediate energies is a powerful tool to probe the nuclear spin response. Due to the energy dependence of the isovector part of the t matrices, the nucleon charge exchange reaction excites predominantly the spin-isospin excitations in nuclei at projectile energies above 100 MeV. As a result, spin excitations are populated strongly in the (p,n) reaction, while the isobaric analog state (IAS) and other non-spin-flip states are relatively weakly.

The most prominent of these spin-isospin excitations is the discovery of the Gamow-Teller (GT) giant resonance [1–6], the spin-isospin collective mode which was predicted by Ikeda, Fujii, and Fujita [7] in 1963. The GT giant resonance appears energetically in the continuum region of the nuclear excitation spectrum. An essential model-independent sum rule (Ikeda's sum rule) exists for the GT transition [7,8]. Surprisingly, less than 2/3 of the minimum GT sum rule value has been experimentally identified from the systematic studies of the (p,n) reaction [9].

Two physically different mechanisms have been proposed for this so-called *quenching* of the total GT strength. One is the $\Delta(1232)$-isobar nucleon-hole (ΔN^{-1}) admixture into the proton-particle neutron-hole $(1p1h)$ GT state resulting in a part of the GT strength being moved from the low excitation region to the Δ excitation region [10–12]. This mechanism invalidates the Ikeda's sum rule which is based on the assumption that a nucleus consists of structureless nucleons. The modified sum rule considering the quark degrees of freedom predicts that the dominant part of the GT strength is carried away by the ΔN^{-1} excitation in the quark model.

The other mechanism for explaining the quenched GT strength is due to the ordinary nuclear configuration mixing [13–15]. The energetically high-lying two-particle two-hole $(2p2h)$ state mixes with the low-lying $1p1h$ GT state and shifts the GT strength in the energy region beyond the GT giant resonance. Bertsch and Hamamoto [15] have pointed out that roughly 50% of the total GT strength could be shifted into the region of $10-45$ MeV excitation. The importance of this effect, however, depends sensitively on the coupling strength between the $1p1h$ and $2p2h$ states. If the nuclear configuration mixing plays an important role, then the quenched GT strength would actually be located in the high excitation region beyond the GT giant resonance. Consequently the GT strength must be identified in the continuum.

A relatively simple relationship between the measured 0° $(L=0)$ cross section and the GT transition strength B(GT) has been derived [3,16]. This relationship has been successfully used to obtain the B(GT) values for the transitions which are energetically inaccessible to β decay. An application of this relationship, however, requires to obtain the $L=0$ component of the cross section in these transitions. At the high excitation region, therefore, a multipole decomposition (MD) technique [17] should be used to obtain the

*Electronic address: wakasa@nucl.phys.s.u-tokyo.ac.jp
†Present address: Advanced Technology Division, O-arai Engineering Center, Power Reactor and Nuclear Fuel Development Corporation, O-arai, Ibaraki 311-13, Japan.
‡Present address: Cyclotron Laboratory, The Institute of Physical and Chemical Research, Wako, Saitama 351-01, Japan.

transition strength with angular momentum transfer $L=0$ since the contribution from the strength with angular momentum transfer $L\geqslant 1$ is not negligible.

In the present study we report measurements of the double differential cross sections at angles $\theta_{\rm lab}$ between 0.0° and 12.3° and polarization transfer D_{NN} at 0° for the ^{90}Zr(p,n) reaction at $T_p=295$ MeV. The incident beam energy of 295 MeV is one of the best energies to study the GT strength since the ratio of the isovector spin-flip interaction strength to the non-spin-flip one is maximum around this incident energy [18]. It should be noted that the effect of distortions becomes minimum around this incident energy. This fact allows us to extract nuclear structure information such as the GT strength reliably by using the (p,n) reaction.

The MD technique is used to analyze the angular distributions of the cross sections and to obtain the $L=0$ cross section. In order to get a reliable result from the MD analysis, the cross section should be dominated by a single collision of the projectile nucleon with the target nucleons. Smith and Wambach [19] have reported that the two-step collision contributes to the cross sections in about half of the total cross sections at an excitation energy of 50 MeV in the case of the ^{90}Zr(p,n) reaction at $T_p=200$ MeV. Recently Watanabe and Kawai have performed the semiclassical distorted wave (SCDW) calculation [20] for the ^{90}Zr(p,n) reaction at $T_p=300$ MeV which predicts the two-step contribution to be less than 10% of the total cross sections at 50 MeV excitation [21]. Therefore the results of the MD analysis would be highly reliable up to around 50 MeV excitation if the measurement was made at $T_p=300$ MeV.

The $L=0$ cross section deduced from the MD analysis is extrapolated to $(q,\omega)=(0,0)$ to obtain the GT transition strength B(GT). The distribution of the GT strength is compared with the perturbative calculation by Bertsch and Hamamoto [15] as well as with the second-order random phase approximation (SRPA) calculation by Drożdż *et al.* [22], both of which treat the mixing of the GT strength with $2p2h$ configurations.

II. EXPERIMENT

A. Proton beam and target

The neutron time-of-flight facility [23] at the Research Center for Nuclear Physics (RCNP) was used for the measurement. A polarized proton beam was accelerated up to a kinetic energy of 295 MeV by using the AVF and RING cyclotrons. A beam pulse selection of 1/4 was applied in the injection line from the AVF to RING cyclotrons, which yields an effective beam pulse separation of about 260 ns. The beam polarization was measured by a beam line polarimeter and it was typically 0.73. The polarimeter consists of two arms of collimated pairs of conjugate-angle plastic-scintillator telescopes that continuously monitor the beam polarization by using the ^{1}H$(\vec{p},p)^1$H reaction with a CH_2 target.

An enriched ^{90}Zr target with a thickness of 112 mg/cm^2 was placed in a beam-swinger dipole magnet. Neutrons from the (p,n) reaction traveled in a 100 m time-of-flight (TOF) tunnel. Protons downstream of the target were swept by the beam-swinger magnet into an electrically isolated graphite beam stop (Faraday cup) connected to a current integrator. The beam line polarimeter was also helpful for monitoring the integrated beam current.

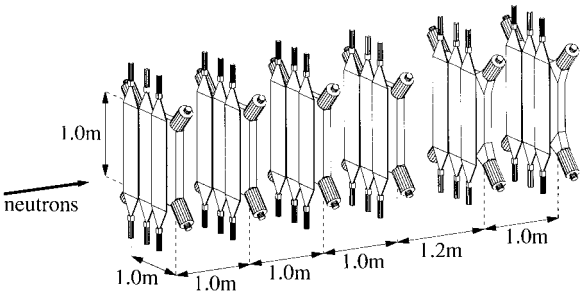

FIG. 1. A schematic view of the NPOL2 system. In the polarimetry mode of NPOL2, one of the five neutron detectors (all except for the last one) serves as a neutron polarization analyzer, and the following neutron detector acts as a catcher of doubly scattered neutrons or recoil protons. Thin plastic scintillation detectors in front of each neutron detector are used to identify charged particles.

B. Neutron detector/polarimeter

Neutrons from the (p,n) reaction were detected by the neutron polarimeter NPOL2 [24]. As illustrated in Fig. 1, the NPOL2 system consists of six planes of two-dimensional position-sensitive neutron detectors. The size of each detector is $1\times1\times0.1$ m^3. The first four detectors are made of liquid scintillator BC519, and the last two detectors are made of plastic scintillator BC408. Each scintillator is viewed from four corners by photo multiplier tubes (PMT's) with radii of 12.7 cm. The two-dimensional positions are reconstructed from the fast timing information derived from PMT's. The position resolutions are about 6 to 10 cm and about 4 to 8 cm for liquid and plastic scintillators, respectively, depending on positions.

Neutron flight time is determined by using timing signals from the PMT's with an rf signal. A prominent γ ray from the decay of π^0 produced in the target provides a convenient time reference for establishing the absolute TOF scale. The absolute neutron energy is determined by using the transitions to discrete states with known reaction Q values. The mean beam energy at the target center was thus determined to be $T_p=295.0\pm1.0$ MeV. The neutron flight path was 100 m for the measurement of the double differential cross sections and was 70 m for the measurement of the $D_{NN}(0°)$ values. The overall energy resolution, including a target energy-loss contribution of about 0.3 MeV, is about 1.9 MeV in full width of half maximum (FWHM).

In the polarimetry mode of NPOL2, one of the five neutron detectors (all except for the last one) serves as a neutron polarization analyzer. The neutron polarization can be obtained utilizing both the ^{1}H$(\vec{n},n)^1$H and ^{1}H$(\vec{n},p)n$ reactions. A kinematical discrimination of the $n+p$ events from the $n+$C events has been made by using time, position, and pulse-height information. This kinematical selection also provides a highly efficient filter against background events from cosmic rays, target γ rays, or the wrap around of slow neutrons from preceding beam pulses. Neutron polarization is determined from the azimuthal distribution of the $n+p$

events. There is a fairly large contribution from the quasifree scattering of the $^{12}C(n,np)$ reaction because the reaction kinematics of the quasifree scattering is very similar to that of the $n+p$ reaction. This contribution might modify the qualitative features (effective analyzing powers and double scattering efficiencies) of the polarimeter system modeled by using the observables of the free nucleon-nucleon (NN) scattering. Therefore we have calibrated the polarimeter system empirically as described in detail below.

III. DATA REDUCTION AND RESULTS

A. Neutron detection efficiency

The relation between the number of measured neutrons $N_{\rm obs}$ and the double differential cross section $d^2\sigma_{\rm lab}/d\Omega dE$ is given by

$$\frac{d^2\sigma_{\rm lab}}{d\Omega dE}=\frac{N_{\rm obs}}{I\rho\Delta\Omega\epsilon T f_{\rm live}}, \tag{1}$$

where I is the number of incident protons, ρ is the target thickness in nuclei/cm^2, $\Delta\Omega$ is the solid angle subtended by the detector (98 μsr), ϵ is the intrinsic detector efficiency for neutrons, T is the transmission factor along the flight path in the air, and $f_{\rm live}$ is the detector live fraction.

Since it is difficult to measure the values ϵ and T independently, we obtained the product of these two values by measuring the neutron yield from the 0° ^{7}Li$(p,n)^7$Be(g.s.+0.43 MeV) reaction, which has a constant center-of-mass cross section of $\sigma_{\rm c.m.}(0°)=27.0\pm0.8$ mb/sr over the wide bombarding energy range from 80 to 795 MeV [25]. This reaction was used to extract ϵT values at bombarding energies of 146, 296, and 392 MeV, which are sufficient to estimate the efficiencies spanning the neutron energy range necessary for the present data analysis. The detection efficiency (ϵT) is found to be almost independent of neutron energy, with a value of approximately 0.15 by combing all of the six neutron detectors. The minor correction for the energy dependence of the detection efficiency has been applied to the present data.

B. Effective analyzing powers

The effective analyzing powers of NPOL2 were calibrated by using polarized neutrons produced by the 0° ^{2}H$(\vec{p},\vec{n})pp$ reaction at $T_p=146$, 296, and 392 MeV ($T_n=141$, 291, and 387 MeV). The polarization transfer coefficients $D_{LL}(0°)$ of the ^{2}H$(\vec{p},\vec{n})pp$ reaction at $T_p=305$ through 788 MeV were measured by McNaughton *et al.* [26]. At 0°, polarization transfer coefficients satisfy the following relation [27,28]:

$$D_{LL}(0°)+2D_{NN}(0°)+1=0.$$

From this relation we can deduce the $D_{NN}(0°)$ values at $T_p=296$ and 392 MeV. At $T_p=146$ MeV, we have used the $D_{NN}(0°)$ value at $T_p=141$ MeV predicted by Bugg and Wilkin [27]. It should be noted that the polarization transfer $D_{NN}(0°)$ of this reaction at $T_p=160$ MeV was measured by Sakai *et al.* [29]. The result is -0.43 ± 0.04, which is consistent with the theoretical prediction. A detailed report concerning the calibration and operation of the polarimeter system will be given in the forthcoming paper [30]. In the following paragraph, therefore, we present a brief description of the performance of NPOL2.

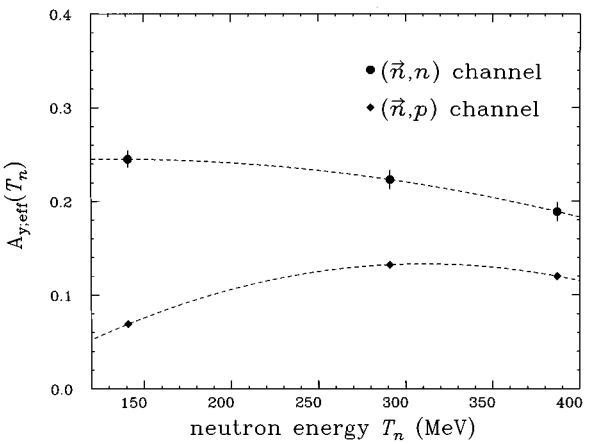

FIG. 2. Effective analyzing powers of NPOL2 in the $(\vec{n},n)$ (filled circles) and $(\vec{n},p)$ (filled diamonds) reaction channels. The dashed curves are the results of the fitting by using second order polynomial functions.

Figure 2 shows the effective analyzing powers as a function of neutron kinetic energy. Typical statistical uncertainties are about 0.010 and 0.004 for the $(\vec{n},n)$ and $(\vec{n},p)$ channels, respectively. The systematic uncertainty comes mainly from the uncertainty of the incident proton polarization (1%) and from the uncertainty of the polarization transfer $D_{NN}(0°)$ (1–2 %). It is interesting to note that effective analyzing powers for the $(\vec{n},p)$ channel have fairly large and almost constant values of about 0.1 over the neutron kinetic energy region from $T_n=200$ to 400 MeV. The performance of a polarimeter is characterized by a figure of merit (FOM) defined by FOM $=\epsilon_{\rm DS}A_{y;\rm eff}^2$, where $\epsilon_{\rm DS}$ is a double scattering efficiency. The total [$(\vec{n},n)$ and $(\vec{n},p)$ channels] FOM values of NPOL2 are 1.1×10^{-4}, 3.9×10^{-4}, and 4.3×10^{-4} at $T_n=141$, 291, and 387 MeV, respectively. These values can be compared with that of the NTOF polarimeter at LAMPF reported as 2.1×10^{-4} at $T_n=313$ MeV [31], which is about a half of our FOM value of 3.9×10^{-4} at $T_n=291$ MeV.

C. Cross sections

The double differential cross sections as a function of scattering angle and excitation energy are shown in Fig. 3 for $\theta_{\rm lab}=0.0°$, 0.7°, 2.3°, 4.6°, 7.0°, 9.8°, and 12.3°. In addition to the statistical uncertainty, there is about 2% uncertainty in the determination of the integrated current for each angle. The systematic uncertainty of the normalization in the cross section also includes the uncertainties both of the ^{7}Li cross section (3%) and of the target thickness (3%). These uncertainties, however, have little effect on the multipole decomposition analysis described below since they are common to all angles.

The main feature of the 0° spectrum is the discrete peak at $E_x=2.3$ MeV and the GT giant resonance at $E_x\approx9$ MeV, while the dipole resonance at $E_x\approx18$ MeV is relatively en-

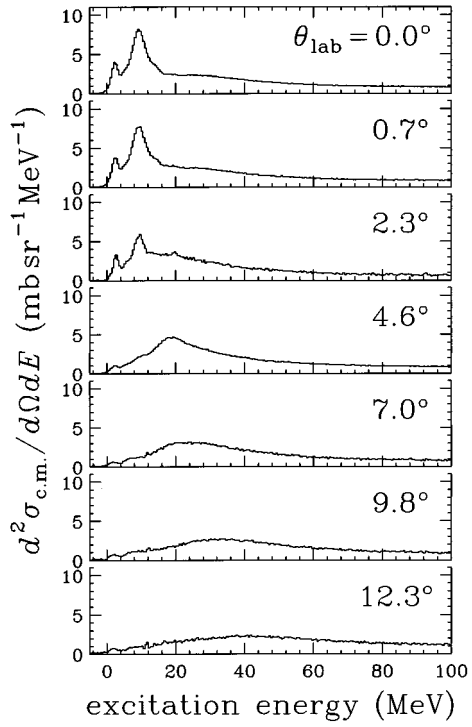

FIG. 3. Differential cross sections for the ^{90}Zr$(p,n)^{90}$Nb reaction at T_p=295 MeV.

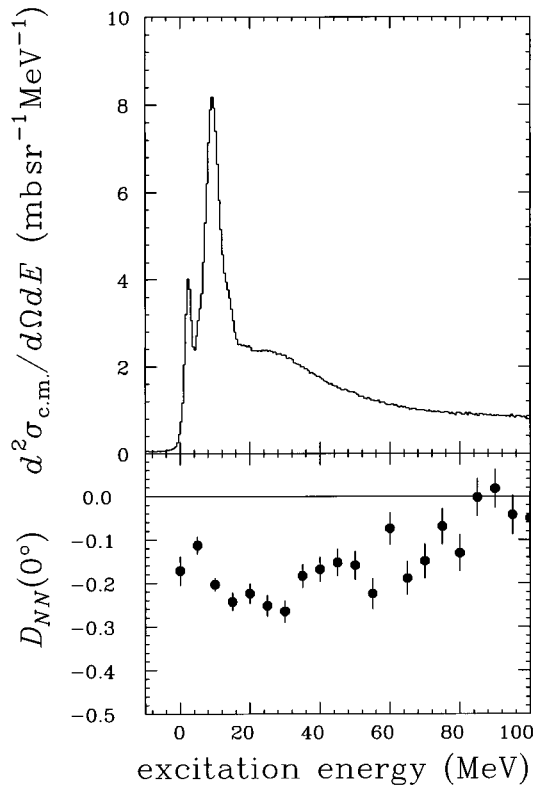

FIG. 4. Excitation energy spectra for the cross section and polarization transfer D_{NN} for the ^{90}Zr$(p,n)^{90}$Nb reaction at T_p = 295 MeV and at 0°.

hanced at $\theta_{\rm lab}$ = 4.6°. The 0^+ IAS at E_x=5.1 MeV does not form any peak structure. The Fermi transition is strongly suppressed relative to the GT transition in this incident energy region since the ratio of the GT unit cross section to the Fermi unit cross section takes a value as large as 14.7 ± 1.1 at T_p=300 MeV [18]. The present energy resolution of 1.9 MeV in FWHM does not allow us to separate the small contributions due to the excitations at E_x=1.0 and 3.0 MeV from the excitation at E_x=2.3 MeV.

D. Polarization transfer $D_{NN}(0°)$

Figure 4 shows the double differential cross section and polarization transfer D_{NN} at 0° as a function of excitation energy. The data of the $D_{NN}(0°)$ values in this figure have been sorted into an excitation energy bin of 5 MeV width to reduce statistical fluctuations. An interesting feature is the large negative $D_{NN}(0°)$ values up to 60 MeV excitation. This large negative $D_{NN}(0°)$ value, which is not observed in the study at 160 MeV [32], indicates strongly the existence of spin-flip strength.

IV. ANALYSIS

In this section we present theoretical analyses including the results of a multipole decomposition analysis.

A. Theoretical calculations for $D_{NN}(0°)$

In a plane wave impulse approximation (PWIA), a nucleon-nucleus scattering amplitude is described as a product of the nuclear transition density and the *NN* scattering amplitude which may either be represented as [33]

$$M(q)=A+B\sigma_{1n}\sigma_{2n}+C(\sigma_{1n}+\sigma_{2n})+E\sigma_{1q}\sigma_{2q}+F\sigma_{1Q}\sigma_{2Q}, \tag{2}$$

or alternatively as a sum of central, spin-orbit, and tensor terms:

$$M(q)=A+\frac{1}{3}(B+E+F)\boldsymbol{\sigma_1}\cdot\boldsymbol{\sigma_2}+C(\boldsymbol{\sigma_1}+\boldsymbol{\sigma_2})\cdot\hat{\mathbf{n}}+\frac{1}{3}(E-B)S_{12}(\hat{\mathbf{q}})+\frac{1}{3}(F-B)S_{12}(\hat{\mathbf{Q}}), \tag{3}$$

where S_{12} is the usual tensor operator [34] and

$$\hat{\mathbf{q}}=\frac{\mathbf{k}_f-\mathbf{k}_i}{|\mathbf{k}_f-\mathbf{k}_i|}\ , \quad \hat{\mathbf{Q}}=\frac{\mathbf{k}_i+\mathbf{k}_f}{|\mathbf{k}_i+\mathbf{k}_f|},$$

and

$$\hat{\mathbf{n}}=\hat{\mathbf{Q}}\times\hat{\mathbf{q}}.$$

If a single L transfer is dominant, the $D_{NN}(0°)$ value for the GT transition is given by [35]

$$D_{NN}(0°)=\frac{-F^2}{F^2+2B^2}. \tag{4}$$

Therefore the polarization transfer $D_{NN}(0°)$ is only sensitive to the effective *NN* interaction and could offer a convenient means of selecting the adequate *NN* interaction used in a

distorted wave impulse approximation (DWIA) calculation. It should be noted that the deviation of the $D_{NN}(0°)$ value from $-1/3$ is due to the contribution from the exchange tensor $S_{12}(\hat{\mathbf{Q}})$ interaction [36].

We have performed DWIA calculations by using the computer code DW81 [37] to obtain the $D_{NN}(0°)$ values for the GT transitions. The knock-on exchange amplitude is treated exactly in this code. Optical potential parameters are needed to calculate the distortions in the incident and outgoing channels. The optical potential parameters for incident protons are taken from Ref. [38]. The optical potential parameters for outgoing neutrons are taken from Ref. [39], in which the neutron relativistic optical potentials have been presented for various nuclei from C to U with neutron kinetic energies of $T_n = 20 \sim 1000$ MeV. These neutron optical potentials depending on the neutron kinetic energy are suitable for the present DWIA calculation concerning the wide excitation region of ^{90}Nb. Therefore we can take account of changes of distortions in the outgoing channel as a function of neutron kinetic energy . The one-body density matrix elements (OBDME) for the GT transitions of the ^{90}Zr$(p,n)^{90}$Nb reaction were obtained from Ref. [40]. This shell-model calculation was performed in the $(p_{1/2}g_{9/2})^{14}$ $+(p_{1/2}g_{9/2})^{13}(g_{7/2}d_{5/2}d_{3/2}s_{1/2})$ configurations by using phenomenological effective interactions. The single particle radial wave functions were assumed to have a harmonic oscillator (HO) shape with a range parameter $b = 2.12$ fm [34]. It should be noted that DWIA calculations and associated $D_{NN}(0°)$ values are relatively insensitive both to the detailed shapes of radial wave functions and to the choice of optical potentials [36]. The effective NN interaction was taken from the t-matrix parametrization of the free NN interaction by Franey and Love [41]. The DWIA calculations were done for the t-matrix parametrizations at 270 and 325 MeV.

The results of the DWIA calculations are shown in Fig. 5, in which the data of the $D_{NN}(0°)$ values have been sorted into excitation energy bins of 2 MeV width. The 0^+ ($L=0$, $S=0$) IAS transition at $E_x=5.1$ MeV, for which the $D_{NN}(0°)$ value takes a value of 1, stands out clearly in the spectrum of $D_{NN}(0°)$. The dashed and solid curves correspond to the calculations using the t-matrix parametrizations at 270 and 325 MeV, respectively. The calculated cross sections and polarization transfer $D_{NN}(0°)$ have been folded with a Gaussian distribution of 1.9 MeV FWHM to simulate the experimental energy resolution. It is found that the calculated cross section by using the 325 MeV t-matrix parametrization needs a normalization factor of 0.57 to reproduce the measured 0° cross section for the discrete GT state at $E_x=2.3$ MeV. This normalization factor has been applied to both calculated cross sections shown in Fig. 5. The origin of this normalization factor might be due to the coupling of the GT state with high-lying $2p2h$ and/or ΔN^{-1} excitations. The theoretically obtained width of the GT giant resonance peak is only about a half of the experimentally observed width, which is mainly due to the limited configurations included in the shell-model calculation.

The cross sections in DWIA calculations are quite similar with one another meaning the insensitivity of the cross sections to the effective interaction. The polarization transfer $D_{NN}(0°)$, on the contrary, is very sensitive to the choice of

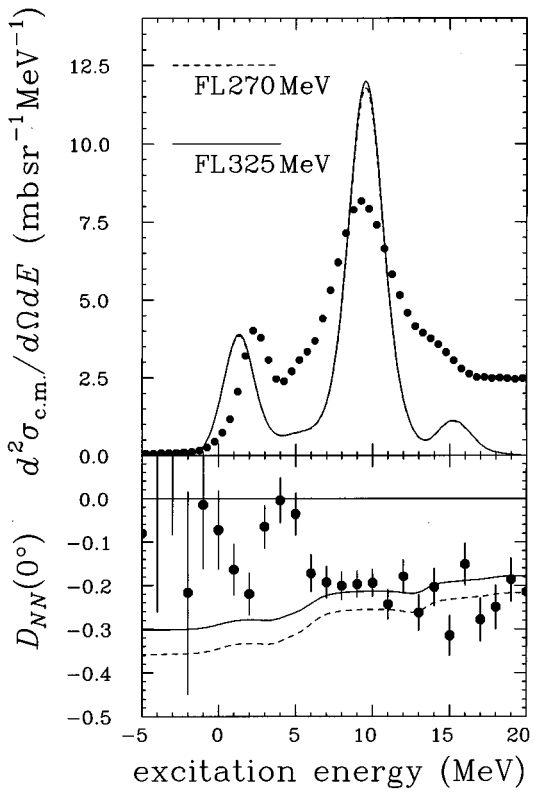

FIG. 5. Excitation energy spectra of the cross section and polarization transfer D_{NN} at 0° in the GT giant resonance region. The dashed and solid curves correspond to the results of DWIA calculations using the t-matrix parametrization of Franey and Love at 270 and 325 MeV, respectively. See text for details.

the t-matrix parametrization. An excellent agreement with the data is obtained by using the 325 MeV parametrization for the GT giant resonance region ($6 \leqslant E_x \leqslant 10$ MeV). We, therefore, use the t-matrix parametrization at 325 MeV in the following DWIA calculations.

B. Theoretical calculations for the low-lying GT states

The DWIA calculations have been performed for the 1^+ state at $E_x=2.3$ MeV. The purpose of these calculations is mainly to confirm the reliability of the parameters used in DWIA calculations. The optical model parameters and the range parameter of the HO radial wave functions are the same as those used in the previous calculations for the polarization transfer $D_{NN}(0°)$. The OBDME is taken from the shell-model calculation of Ref. [40], which predicts 14 GT states up to 4.0 MeV excitation of ^{90}Nb. It is interesting to note that both plane-wave impulse approximation (PWIA) and DWIA calculations give almost identical shapes of angular distributions in the measured angular range, clearly indicating low sensitivity to different sets of optical potentials. Calculations were also done in which single particle radial wave functions were generated from a Woods-Saxon (WS) potential, the depth of which was adjusted to reproduce the binding energy. The binding energies of neutrons and protons were obtained from the experimental data of the ^{90}Zr$(p,d)^{89}$Zr [42] and ^{90}Zr$(d,n)^{91}$Nb [43] reactions, respectively. Unbound single particle states were assumed to

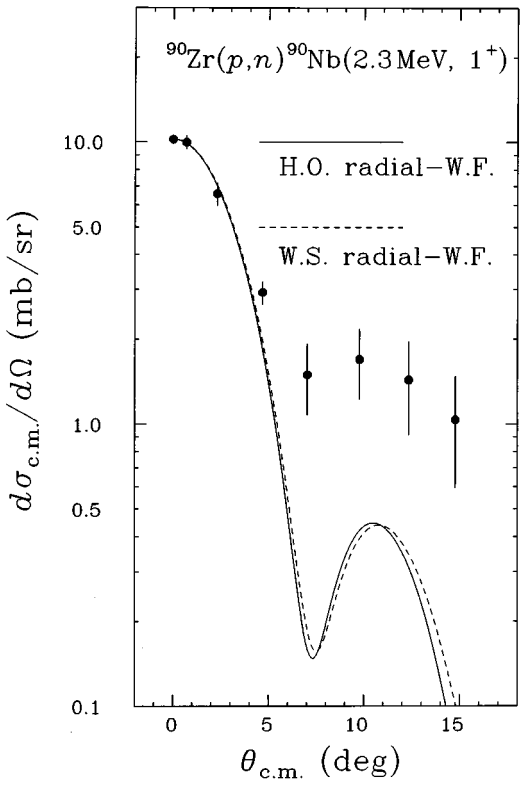

FIG. 6. Measured angular distribution for the neutron group at E_x=2.3 MeV in ^{90}Nb excited via the ^{90}Zr$(p,n)^{90}$Nb reaction at T_p=295 MeV (filled circles with 1σ error bars). The curves are DWIA calculations corresponding to the sum of 14 GT 1$^+$ transitions up to 4.0 MeV of excitation in ^{90}Nb. The results of DWIA calculations shown in this figure have been normalized by a factor of 0.57 to reproduce the measured 0° cross section. See text for details.

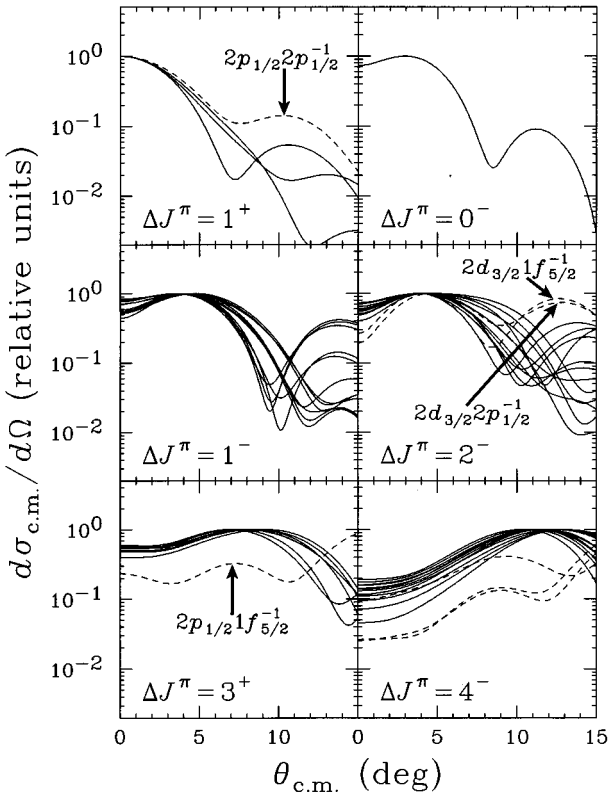

FIG. 7. Arbitrarily normalized distorted wave differential cross sections of the indicated J^π transitions for various $1p1h$ configurations. All calculations are presented for an energy loss of 30 MeV.

be a shallow binding energy to simplify the calculations. No major changes have been observed for the shapes of the differential cross sections in the calculations performed either with HO or with WS single particle radial wave functions. The shapes of the angular distributions, therefore, are insensitive to details of radial wave functions.

The experimentally observed angular distribution for the peak at E_x=2.3 MeV is shown in Fig. 6 by the filled circles, which has a $L=0$ shape at forward angles. Note that the peak contains the transitions to the states at E_x=1.0 and 3.0 MeV due to the present energy resolution. In Fig. 6, the solid and dashed curves correspond to DWIA calculations using HO and WS radial wave functions, respectively. The calculated differential cross sections are normalized by a factor of 0.57 to reproduce the experimental value of $\sigma_{\rm c.m.}(0°)=10.1\pm0.4$ mb/sr. A fairly good agreement with the measured values is observed in the forward angle. The experimental value starts to deviate from the calculated value for the 1$^+$ transitions at an angle greater than about 5°. This disagreement might arise from the contribution of $L\geqslant1$ components. The differential cross sections of the excited state at E_x= 1.0 MeV in Ref. [2] are indeed almost constant with respect to the scattering angles. The reason of this disagreement in the angular distribution at large angles, therefore, is most likely due to the excited state at E_x=1.0 MeV.

C. Multipole decomposition analysis

The shapes of the empirical angular distributions are characterized by the transferred J^π values. The DWIA calculations, however, reveal that the angular distribution of a differential cross section is mainly characterized by L, and that the difference in shapes among the members ($J=L\pm1$,L) of a given L transfer is small in the limited angular range such as the case of the present data. Thus we carried out the MD analysis by grouping all J^π transitions to the lowest L value.

We have calculated angular distributions for the following final J^π states: 1$^+$ ($L=0$); 0$^-$, 1$^-$, and 2$^-$ ($L=1$); 3$^+$ ($L=2$); and 4$^-$ ($L=3$). Because of the finite number of the data points in the angle, the J^π states for $L\geqslant2$ transfers are restricted to unnatural parity states. Note that the observed large negative $D_{NN}(0°)$ values up to around 60 MeV excitation indicate the presence of significant strength of unnatural parity states [44]. The difference of the shapes of the angular distributions for several $1p1h$ configurations for a given J^π transfer has been investigated. An active neutron hole is restricted to the $1f_{7/2}$, $1f_{5/2}$, $2p_{3/2}$, $2p_{1/2}$, or $1g_{9/2}$ shell since the ^{40}Ca is assumed to be a core. An active proton particle is restricted to the $2p_{1/2}$, $1g_{9/2}$, $1g_{7/2}$, $2d_{5/2}$, $2d_{3/2}$, $1h_{11/2}$, or $3s_{1/2}$ shell. Calculated shapes of the angular distributions for an excitation energy of 30 MeV are shown in Fig. 7 for all possible $1p1h$ configurations within these active neutron and proton shells. The figure clearly shows that the shapes in the angular range considered here are almost independent of the assumption of the $1p1h$ configura-

tion. Some exceptions, however, can be found. For example, (1) The $2p_{1/2}2p_{1/2}^{-1}$ configuration for the $J^\pi=1^+$ transition has a fairly large second maximum at about $\theta_{\text{c.m.}}=8°$. (2) The $2d_{3/2}1f_{5/2}^{-1}$ and $2d_{3/2}2p_{1/2}^{-1}$ configurations for the $J^\pi=2^-$ transition have fairly large second maxima at about $\theta_{\text{c.m.}}=12°$. (3) The $1f_{5/2}2p_{1/2}^{-1}$ configuration for the $J^\pi=3^+$ transition peaks at around $\theta_{\text{c.m.}}=16°$ whereas other $1p1h$ configurations peak at around $\theta_{\text{c.m.}}=8°$. These exceptions show the common characteristic feature; transitions with $J^\pi=1^+$, 2^-, and 3^+ have large contributions from the angular momentum transfers with $L=2$, 3, and 4 rather than those with $L=0$, 1, and 2, respectively.

For each 1.0 MeV excitation energy interval, the experimentally obtained angular distribution $\sigma^{\text{exp}}(\theta_{\text{c.m.}},E_x)$ was fitted by means of the least square method with the sum of calculated angular distributions $\sigma_{J^\pi}^{\text{calc}}(\theta_{\text{c.m.}},E_x)$ weighted with fitting coefficients a_{J^π} as

$$\sigma^{\text{exp}}(\theta_{\text{c.m.}},E_x)=\sum_{J^\pi} a_{J^\pi}\sigma_{J^\pi}^{\text{calc}}(\theta_{\text{c.m.}},E_x). \tag{5}$$

The fitting procedure has been performed for all possible 80 640 combinations of the previously calculated angular distributions at each excitation energy from -5 through 70 MeV. Note that the configurations with unusual angular shapes are, of course, included in the calculations. The combination of calculated angular distributions giving the minimum chi-square value was chosen. Although the data are available in 0.5 MeV energy intervals, the choice of 1.0 MeV intervals provides a smoother fit and is good enough to distinguish each L contribution to the cross sections.

Figure 8 shows the result of the MD analysis which is in excellent agreement with the measured cross sections for the whole excitation energy region of all angles. The present MD analysis clearly shows a fairly large contribution of the $L=0$ component up to 50 MeV excitation. The $L=0$ cross section becomes zero around an excitation energy of 70 MeV. We have also carried out the MD analysis by using the angular distributions obtained in DWIA calculations with WS radial wave functions as well as by using the angular distributions obtained in PWIA calculations with HO radial wave functions. The results for the $L=0$ cross section at 0.0° are shown in Fig. 9. The MD analysis is found to be almost independent of the parameters used in DWIA calculations to generate angular distributions up to 50 MeV excitation. However, the $L=0$ cross section at excitation energies larger than 50 MeV seems to be sensitive to the choice of the angular distributions used in the MD analysis, depending on either PWIA or DWIA. Therefore the GT strength described below is discussed by separating the excitation energy region of ^{90}Nb into two regions, (a) $E_x \leqslant 50$ MeV and (b) $E_x > 50$ MeV, to avoid the systematic uncertainty of the B(GT) values coming from the ambiguity of the results in the MD analysis.

V. DISCUSSION

A. GT strength

The $L=0$ cross section $\sigma_{L=0}(q,\omega)$ at low momentum transfer can be related to the corresponding B(GT) value as [16]

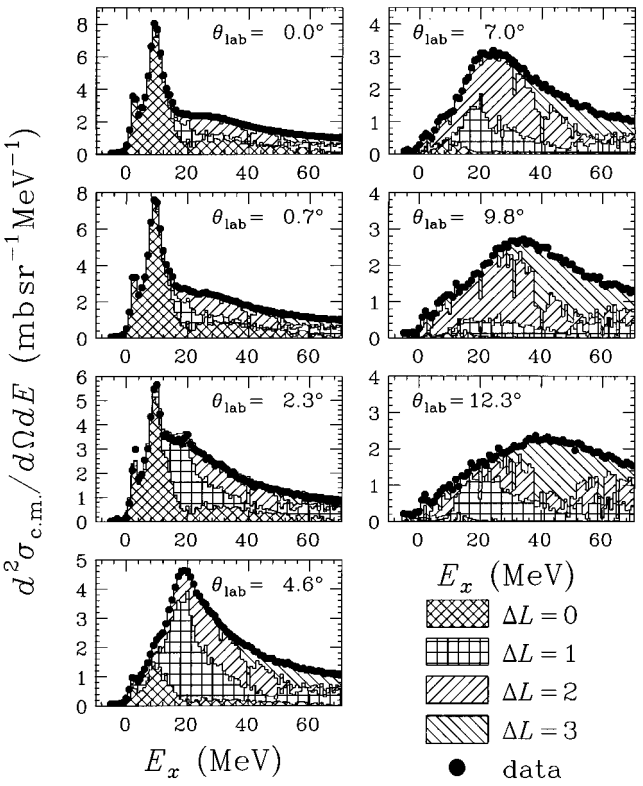

FIG. 8. Results of the multipole decomposition analysis at the indicated angles.

$$\sigma_{L=0}(q,\omega)=\hat{\sigma}_{\text{GT}}F(q,\omega)B(\text{GT}), \tag{6}$$

where $\hat{\sigma}_{\text{GT}}$ is the GT unit cross section and $F(q,\omega)$ describes the dependence on momentum transfer q and energy loss ω. The latter factor is defined to be unity at $(q,\omega)=(0,0)$, and may be expressed as [16]

$$F(q,\omega)=\frac{\sigma_{L=0}(q,\omega)}{\sigma_{L=0}(q=\omega=0)} =\frac{K(T_p,\omega)}{K(T_p,0)}\exp\left(-\frac{1}{3}q^2b\right)\exp[\zeta(\omega)], \tag{7}$$

where K is a kinematic factor, b is a parameter describing the dependence on the momentum transfer, and $\zeta(\omega)$ is a polynomial function describing the dependence on the energy loss as

$$\zeta(\omega)=\sum_{i=1} \alpha_i\omega^i. \tag{8}$$

For a given energy loss ω_0, the momentum transfer dependence of the cross section at small momentum transfer is a Gaussian function of q (Gaussian approximation):

$$\sigma(q,\omega=\omega_0)\propto\exp\left(-\frac{1}{3}q^2b\right). \tag{9}$$

At $\theta_{\text{lab}}=0.0°$ momentum transfer q is a function of energy loss ω, and here we assumed that the factor $-q^2b/3$ describ-

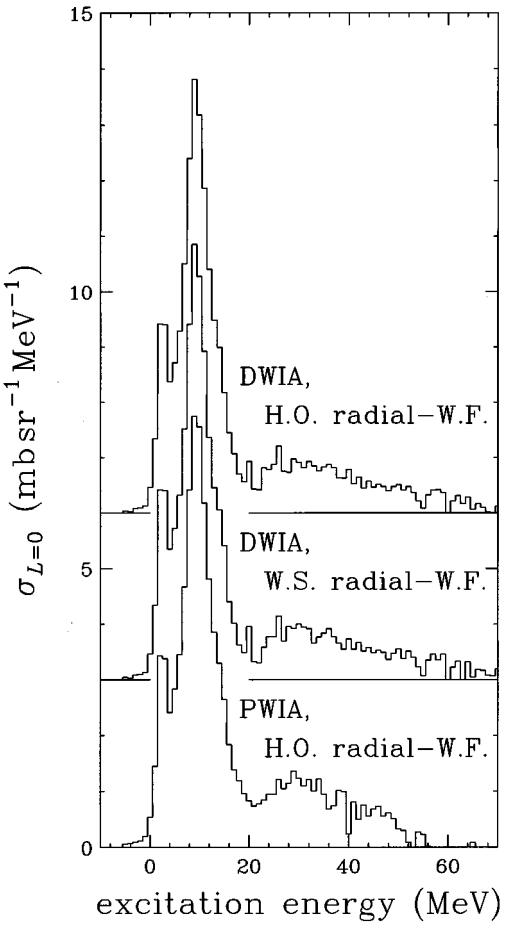

FIG. 9. The $L=0$ cross sections deduced from the MD analysis. The top and middle histograms represent the results of the MD analysis by using the harmonic oscillator and Woods-Saxon radial wave functions in DWIA calculations, respectively. The bottom histogram is the result of the MD analysis by using the angular distribution obtained by the PWIA calculation.

ing the momentum transfer dependence can be expressed as a polynomial function of ω as

$$-\frac{1}{3}q^2b=\sum_{i=1}\beta_i\omega^i\equiv\xi(\omega). \tag{10}$$

The validity of the Gaussian approximation depends not only on the small-q expansion of the central interaction, but also on the assumption that other components of the interaction, such as the tensor force, do not contribute to the cross sections at small momentum transfer [16]. The range of the momentum transfer where these assumptions are valid can be verified by comparing with DWIA calculations. We have performed the DWIA calculations for the GT 1^+ transition to obtain the cross sections as a function of momentum transfer. The calculations were done for the $1g_{9/2}1g_{9/2}^{-1}$, $1g_{7/2}1g_{9/2}^{-1}$, $2p_{1/2}2p_{3/2}^{-1}$, and $2p_{1/2}2p_{1/2}^{-1}$ configurations and the parameters used in DWIA calculations are the same ones used in the previous calculations. It is found that the Gaussian approximation works fairly well up to about $q=0.45$ fm^{-1}. Note that a momentum transfer of 0.45 fm^{-1} corresponds to an excitation energy of about 50 MeV at $\theta_{\rm lab}=0.0°$. Therefore in the extrapolation of the $L=0$ cross section to $q=0$, the contribution of higher-order terms in the small-q expansion not included in the Gaussian approximation is not negligible beyond 50 MeV excitation. In order to extend our analysis beyond 50 MeV excitation, we try to correct the contribution of higher-order terms by adopting an appropriate order of the polynomial function $\zeta(\omega)$, which can be determined by a comparison with DWIA calculations for the $L=0$ transfer as described below.

The energy loss dependence of the cross sections is expressed in Eq. (7) by using the factor $\exp[\zeta(\omega)]$, where $\zeta(\omega)$ is a polynomial function of ω. Because both momentum transfer and energy loss dependence is described by using the polynomial functions of ω, the factor $F(q,\omega)$ can also be expressed by using a polynomial function of ω as

$$F(q,\omega)=\frac{K(T_p,\omega)}{K(T_p,0)}\exp\left(-\frac{1}{3}q^2b\right)\exp[\zeta(\omega)]$$
$$=\frac{K(T_p,\omega)}{K(T_p,0)}\exp[\eta(\omega)], \tag{11}$$

with

$$\eta(\omega)\equiv\xi(\omega)+\zeta(\omega). \tag{12}$$

The order of the polynomial function $\eta(\omega)$ and the magnitude of the polynomial function coefficients can be determined by comparison with DWIA calculations. The quantity

$$F(q,\omega)=\frac{\sigma_{L=0}(q,\omega)}{\sigma_{L=0}(q=\omega=0)}\left(=\frac{K(T_p,\omega)}{K(T_p,0)}\exp[\eta(\omega)]\right), \tag{13}$$

is plotted in Fig. 10. The filled circles, open circles, filled squares, and open squares are the results of DWIA calculations for the $1g_{9/2}1g_{9/2}^{-1}$, $1g_{7/2}1g_{9/2}^{-1}$, $2p_{1/2}2p_{3/2}^{-1}$, and $2p_{1/2}2p_{1/2}^{-1}$ configurations, respectively. A fourth order polynomial function

$$\eta(\omega)=\sum_{i=1}^{4}\gamma_i\omega^i, \tag{14}$$

is found sufficient to fit the calculated ω dependence. The dashed curves show the results of fitting by assuming an energy loss dependence in Eqs. (13) and (14), which reproduce the calculated values very well up to an energy loss of 70 MeV.

The choice of the GT unit cross section $\hat{\sigma}_{\rm GT}$ is very important since it reflects directly on the sum of the GT strength. In our previous study [45] we used the GT unit cross section of $\hat{\sigma}_{\rm GT}=4.3\pm0.3$ mb/sr. This value has been derived from the GT transition at $E_x=2.3$ MeV, for which the B(GT) value is known from the study of the (p,n) reaction at $T_p=120$ MeV by Bainum *et al.* [2]. Bainum *et al.* used the IAS transition, whose Fermi strength is B(F) $=(N-Z)=10$, to normalize the 0° cross section. The normalized cross section was used to deduce the GT strength by using the ratio R^2 of the GT unit cross section relative to

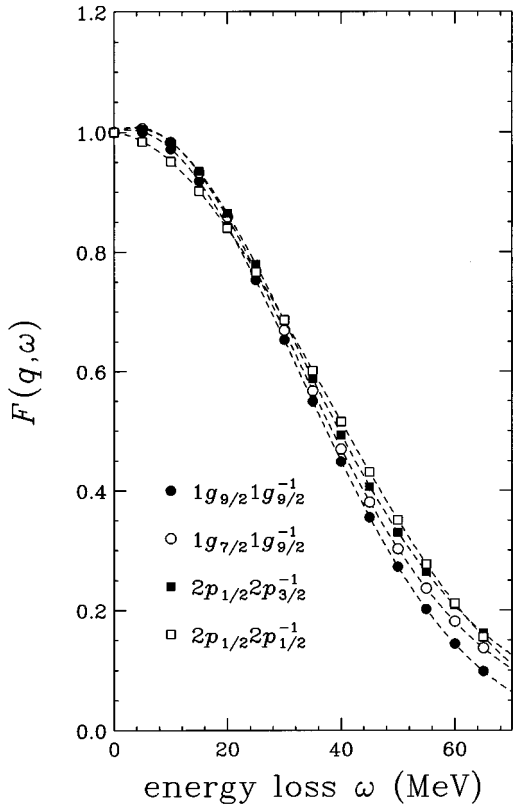

FIG. 10. The factor $F(q,\omega)$ describing momentum transfer and energy loss dependence of the cross sections for the $J^\pi=1^+$ transition deduced from DWIA calculations. The filled circles, open circles, filled squares, and open squares are the DWIA calculations of the $\sigma(q,\omega)/\sigma(q=\omega=0)$ values for the $1g_{9/2}1g_{9/2}^{-1}$, $1g_{7/2}1g_{9/2}^{-1}$, $2p_{1/2}2p_{3/2}^{-1}$, and $2p_{1/2}2p_{1/2}^{-1}$ configurations, respectively. The dashed curves show the results of fitting by assuming the energy loss dependence of Eqs. (11), (12), and (14).

the Fermi unit cross section. They reported the 0° cross section of the IAS transition to be 6.0 ± 0.7 mb/sr, which disagrees with the 4.7 ± 0.4 mb/sr at $T_p=120$ MeV reported by Taddeucci *et al.* [16]. This disagreement might be due to the ambiguity of the background subtraction in the case of Bainum *et al.* Therefore the GT strength reported in Ref. [2] may be inadequate for the derivation of the GT unit cross section.

In the present study we use the B(GT) value reported by Gaarde [9]. He systematically studied the GT unit cross sections as a function of target mass number at $T_p=160$ MeV, and deduced the B(GT) values for various nuclei. In the ^{90}Zr(p,n) case, the sum of the B(GT) values (S_{β^-}) up to the GT giant resonance region was reported to be $S_{\beta^-}=18.3\pm3.0$. From the present MD analysis, we have obtained the $L=0$ cross section up to the GT giant resonance region ($E_x<16$ MeV) to be 67.9 ± 0.2 mb/sr after correcting the momentum transfer and energy loss dependence. The obtained $L=0$ cross section includes the contribution from the IAS transition. Because the R^2 value is 14.7 ± 1.1 at $T_p=300$ MeV [18], the cross section of IAS with the Fermi strength of B(F)=10 can be expressed as

$$\sigma_{\rm IAS}=\hat{\sigma}_{\rm F}F(q,\omega)B({\rm F})=\frac{\hat{\sigma}_{\rm GT}}{R^2}F(q,\omega)B({\rm F})$$
$$=\hat{\sigma}_{\rm GT}F(q,\omega)(0.71\pm0.05). \quad (15)$$

Therefore, the IAS transition contributes little to the GT strength as B(GT)=0.7. The GT unit cross section can be deduced as follows:

$$\hat{\sigma}_{\rm GT}=\frac{\sigma_{L=0}/F(q,\omega)}{B({\rm GT})}=\frac{67.9\pm0.2\ \ {\rm mb/sr}}{(18.3\pm3.0)+(0.71\pm0.05)}$$
$$=3.6\pm0.6\ \ {\rm mb/sr}. \quad (16)$$

The GT unit cross section can also be estimated theoretically from the results of DWIA calculations for the GT 1^+ transition. By using OBDME for the GT 1^+ transition which corresponds to a GT transition strength of B(GT)=1, the cross section at $q=\omega=0$ in the DWIA calculation becomes the GT unit cross section. We have obtained the DWIA calculated values for the GT unit cross section to be $\hat{\sigma}_{\rm GT}=3.7$, 3.4, 2.9, and 3.0 mb/sr for the $1g_{9/2}1g_{9/2}^{-1}$, $1g_{7/2}1g_{9/2}^{-1}$, $2p_{1/2}2p_{3/2}^{-1}$, and $2p_{1/2}2p_{1/2}^{-1}$ configurations, respectively. Thus, the $\hat{\sigma}_{\rm GT}$ value of 3.6 ± 0.6 mb/sr chosen in the present study agrees fairly well with that derived from DWIA calculations.

It is interesting to note that the consistent $\hat{\sigma}_{\rm GT}$ value can be deduced by combining the data for the ^{90}Zr$(p,n)^{90}$Nb reaction at 120 MeV by Bainum *et al.* [2] and Taddeucci *et al.* [16]. Bainum *et al.* reported the cross sections for low lying 1^+ states at $E_x=1.0$, 2.3, and 3.0 MeV as $\sigma_{\rm c.m.}(0°)=0.8\pm0.3$, 5.0 ± 0.5, and 0.9 ± 0.3 mb/sr, respectively. As described in Ref. [2] the state at $E_x=1.0$ MeV is not completely a 1^+ state. Here, however, we assume that the 0° cross section at $E_x=1.0$ MeV is fully coming from the 1^+ component. Then the total cross section of low-lying 1^+ states becomes $\sigma_{1^+}(0°)=6.7\pm0.6$ mb/sr. The ratio R^2 of the GT unit cross section relative to the Fermi unit cross section at 120 MeV can be deduced as [16]

$$R^2(T_p=120\ \ {\rm MeV})=\left(\frac{120\ \ {\rm MeV}}{55\ \ {\rm MeV}}\right)^2=4.76. \quad (17)$$

If we use the cross section for the IAS transition reported by Taddeucci *et al.* [16], the B(GT) value for the low-lying GT 1^+ states is found to be

$$B({\rm GT})=\frac{\sigma_{1^+}(0°)}{\sigma_{\rm IAS}(0°)}\frac{B({\rm F})}{R^2}$$
$$=3.0\pm0.4. \quad (18)$$

In the present experiment at $T_p=295$ MeV, the 0° cross section at $E_x=2.3$ MeV is $\sigma_{\rm c.m.}(0°)=10.1\pm0.4$ mb/sr, which contains the contributions of the transitions to the states at $E_x=1.0$ and 3.0 MeV due to the present energy resolution. Therefore the GT unit cross section at $T_p=295$ MeV can be deduced as

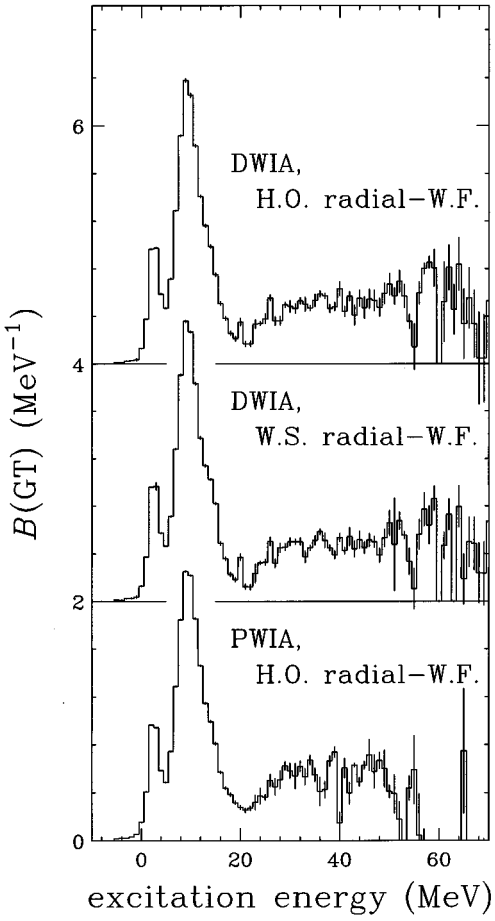

FIG. 11. Gamow-Teller strength distribution obtained from the $0°$ $L=0$ cross section which is deduced from the MD analysis. The top histogram represents the GT strength deduced from the results of the MD analysis by using the angular distributions obtained in the DWIA calculations with HO radial wave functions. The middle histogram represents the GT strength deduced from the results of the MD analysis by using the angular distributions obtained in the DWIA calculations with WS radial wave functions. The bottom histogram represents the GT strength deduced from the results of the MD analysis by using the angular distributions obtained in the PWIA calculations with HO radial wave functions.

$$\hat{\sigma}_{\mathrm{GT}}=\frac{\sigma_{\mathrm{c.m.}}(0°)}{B(\mathrm{GT})}$$
$$=3.4\pm0.1\pm0.4 \quad \mathrm{mb/sr}, \tag{19}$$

where the first uncertainty comes from the statistical uncertainty of the cross section and the second uncertainty is originating from the uncertainty of the $B(\mathrm{GT})$ value. In these calculations we neglect the momentum transfer and energy loss correction factor $F(q,\omega)$ since the $F(q,\omega)$ value is close to unity in the low excitation region. This $\hat{\sigma}_{\mathrm{GT}}$ value of 3.4 mb/sr is consistent with the adopted $\hat{\sigma}_{\mathrm{GT}}$ value of 3.6 ± 0.6 mb/sr in the present study.

Now we have fixed all of the parameters which are necessary to derive the $B(\mathrm{GT})$ values from the $\sigma_{L=0}(q,\omega)$ values. Figure 11 shows the $B(\mathrm{GT})$ values obtained from the the MD analysis as a function of excitation energy. A striking feature is the fairly large and constant $B(\mathrm{GT})$ values of about 0.45 MeV^{-1} up to 50 MeV excitation. We have also obtained the $B(\mathrm{GT})$ values derived from the results of the MD analysis by using the angular distributions obtained in the DWIA calculations with WS radial wave functions as well as by using the angular distributions of the PWIA calculations with HO radial wave functions. Both of the results are also shown in Fig. 11 as a function of excitation energy. Because the results of the MD analyses are almost independent of the parameters used in the DWIA calculations to generate the angular distributions up to 50 MeV excitation, the $B(\mathrm{GT})$ values deduced from the $L=0$ cross section are also insensitive to the parameters used in the DWIA calculations. The $B(\mathrm{GT})$ values beyond 50 MeV excitation, however, are very sensitive to the choice of parameters used in the DWIA calculations. Figure 12 shows the accumulated sum of $B(\mathrm{GT})$ values as a function of excitation energy to clarify the sensitivity of $B(\mathrm{GT})$ values for different parameter sets in the DWIA calculations. The solid, dotted, and dashed curves are the accumulated sum of $B(\mathrm{GT})$ values deduced from the results of the MD analysis by using the angular distributions of the DWIA calculations with HO radial wave functions, those with WS radial wave functions, and those of the PWIA calculations with HO wave functions, respectively. It is found that the sum of $B(\mathrm{GT})$ values up to 50 MeV excitation is insensitive to the parameters used in the calculations and its value varies only within 1.3. The sum of $B(\mathrm{GT})$ values beyond 50 MeV excitation, on the contrary, is very sensitive to the choice of parameters, and its value changes from 2.4 to 9.8. It should be noted that these values are the sum of $B(\mathrm{GT})$ values in the region from 50 to 70 MeV excitation since the $L=0$ cross section in the present MD analysis becomes zero around 70 MeV excitation. Because of the uncertainty involved in the MD analysis, it is

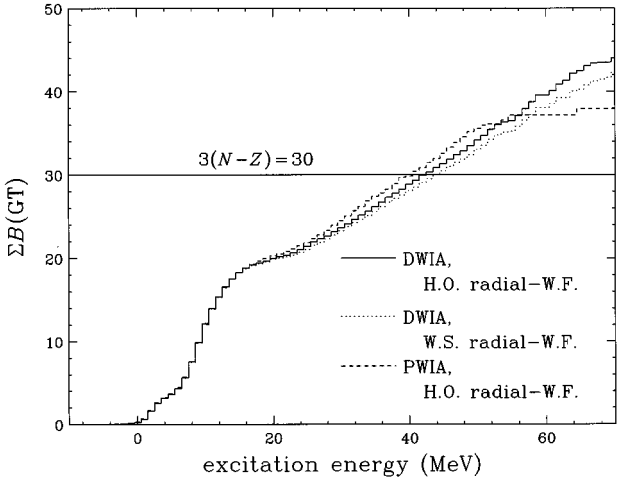

FIG. 12. Sum of GT strength as a function of excitation energy. The solid curve represents the sum of GT strength deduced from the results of the MD analysis by using the angular distributions obtained in the DWIA calculations with HO radial wave functions. The dotted curve represents the sum of GT strength deduced from the results of the MD analysis by using the angular distributions obtained in the DWIA calculations with WS radial wave functions. The dashed curve represents sum of the GT strength deduced from the results of the MD analysis by using the angular distributions obtained in the PWIA calculations with HO radial wave functions.

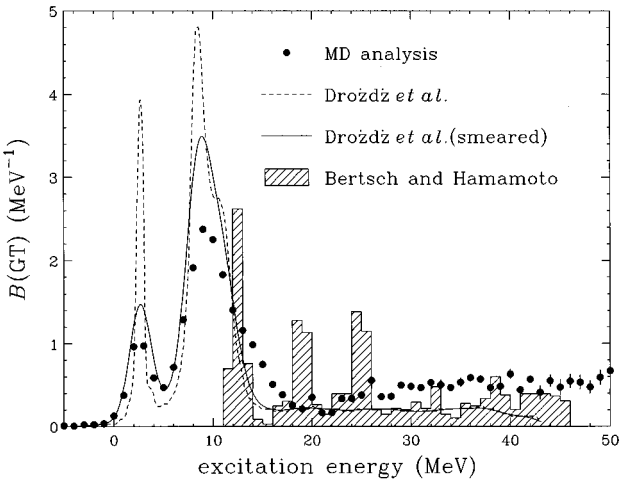

FIG. 13. Gamow-Teller strength distribution (filled circles) obtained from the 0° $L=0$ cross section which is deduced from the MD analysis. The dashed curves and hatched histogram represent the SRPA calculation by Drożdż *et al.* [22] and the perturbative calculation by Bertsch and Hamamoto [15], respectively. The SRPA calculation smeared out to reproduce the experimentally obtained width of the GT transition at $E_x=2.3$ MeV is shown by the solid curve.

very difficult to quote the error in this region. We feel that the sum of B(GT) values beyond 50 MeV excitation could take any value between 0 and 10. In the following discussion, therefore, the GT strength distribution as well as the total GT strength are presented without regard for the GT strength in this region.

In Fig. 13 the perturbative calculation by Bertsch and Hamamoto [15], and the SRPA calculation by Drożdż *et al.* [22] are presented by the hatched histogram and dashed curve, respectively, both of which have taken account of the mixing of the GT strength with $2p2h$ configurations. The B(GT) values deduced from the results of MD analysis using the angular distributions obtained in the DWIA calculations with HO wave functions are also shown in Fig. 13 by the filled circles. The B(GT) values by the SRPA calculation have been folded using a Gaussian distribution to reproduce the width of the GT transition at $E_x=2.3$ MeV, and they are shown by the solid curve in Fig. 13. The centroid energies and widths both of the low-lying GT state at $E_x=2.3$ MeV and of the GT giant resonance are reproduced fairly well by the SRPA calculation. However, the SRPA prediction of about 0.2 MeV^{-1} underestimates the GT strength in the continuum. The perturbative calculation by Bertsch and Hamamoto, on the contrary, agrees with the experimentally obtained value in the continuum. The obtained GT strength in the continuum region of excitation energies between 20 and 50 MeV is 0.45 MeV^{-1}, which is roughly consistent with the theoretical prediction of 0.48 MeV^{-1} [15].

The total experimentally observed GT strength summed over the region up to 50 MeV excitation becomes $S_{\beta^-}=34.2\pm1.6$, or about (114 ± 5)% of the minimum value of the sum rule $3(N-Z)=30$. The uncertainty contains the uncertainties coming from the fitting uncertainties in the MD analysis originating from the statistical uncertainties in the experimental data (0.3) as well as the previously described ambiguity in the MD analysis (1.3). The systematic uncertainty coming from the uncertainty of the GT unit cross section is estimated to be 5.4. The excess of the GT strength from the minimum sum-rule value of $3(N-Z)=30$ is mainly due to the contribution of the isovector spin-monopole (IVSM) strength which is indistinguishable from the GT strength in the MD analysis. In the following subsection, we present the estimation of the contribution of the IVSM resonance to the GT strength obtained from the MD analysis.

B. Contribution from the isovector spin monopole

The $L=0$ cross section obtained from the MD analysis might also include the contribution from the IVSM resonance which is expected to be at about 35 MeV excitation [46,47]. We have performed a series of DWIA calculations for the IVSM state to estimate the contribution to the $L=0$ cross section at 0°.

The OBDME for the IVSM transition is deduced by following the procedure shown by Condé *et al.* [48]. The calculation has been based on normal mode excitation [49], which is the response to a simple tensor operator $\hat{O}^\dagger_{JM}$ acting on the ground state:

$$|JM\rangle \propto \hat{O}^\dagger_{JM}|0\rangle. \tag{20}$$

This normal mode can be expanded in terms of particle-hole states as

$$|JM\rangle = \sum_{ph} X^{JM}_{ph}[a^\dagger_p a_h]_{JM}|0\rangle, \tag{21}$$

where the amplitudes X^{JM}_{ph} are the reduced matrix elements of the operator $\hat{O}^\dagger_{JM}$ for the transition between the ground state and the $1p1h$ state. X^{JM}_{ph} is normalized as

$$X^{JM}_{ph} = \frac{\langle ph;JM|\hat{O}^\dagger_{JM}|0\rangle}{\sqrt{\sum_{ph}|\langle ph;JM|\hat{O}^\dagger_{JM}|0\rangle|^2}}. \tag{22}$$

The normal modes, defined by Eqs. (21) and (22), can be shown to exhaust the full strength associated with the operator $\hat{O}^\dagger_{JM}$. The multipole operator used for IVSM is

$$\hat{O}^\dagger_{LJ} = r^2[\sigma \otimes Y^{M=0}_{L=0}]_{J^\pi=1^+}\tau_-, \tag{23}$$

and a harmonic oscillator ph basis has been used. In the calculation, the ^{90}Zr ground-state wave function is assumed to have protons and neutrons filling up to $2p_{1/2}$ and $1g_{9/2}$ shells, respectively. The configuration space for $1p1h$ excitations was restricted to the $2\hbar\omega$ excitation of ^{90}Nb.

The optical potential parameters are the same as used in the previous calculations, and the t-matrix parametrization at 325 MeV by Franey and Love is used for the effective NN interaction. The single particle radial wave functions should be carefully determined for the IVSM state since its radial transition density has a node around the surface [46,47]. Both the amplitude and the shape of the angular distribution are rather sensitive to the choice of the single particle radial

wave functions. Therefore we have used the WS potential to generate single particle radial wave functions.

The DWIA calculation predicts the 0° cross section for the IVSM state at 35 MeV excitation as 9.9 mb/sr. If we subtract this strength from the $L=0$ cross section obtained from the MD analysis, the total GT strength summed over the region up to 50 MeV excitation becomes $S_{\beta^-}=27.8\pm1.6$, or about (93 ± 5)% of the minimum value of the sum rule $3(N-Z)=30$. In the calculation we assume that all of the IVSM strength is concentrated at an excitation energy of 35 MeV. Auerbach and Klein [47] calculated the distribution of the IVSM strength in ^{90}Zr and found that the IVSM strength might be distributed over a wide excitation energy region. We, therefore, estimate the contribution of the IVSM strength to the 0° cross section when the IVSM strength distributes monotonously as a function of excitation energy. The assumption of the monotonous distribution is quite appropriate since the B(GT) values deduced from the present MD analysis are indeed almost constant making a flat continuum. Two different distributions are tried; 25 MeV $\leqslant E_x^{\rm IVSM}\leqslant$45 MeV and 20 MeV$\leqslant E_x^{\rm IVSM}\leqslant$50 MeV. The final results of the total GT strength summed up to 50 MeV excitation after subtracting the contribution of the flat IVSM distribution become $S_{\beta^-}=27.9\pm1.6$ and 28.1 ± 1.6 for 25 MeV $\leqslant E_x^{\rm IVSM}\leqslant$45 MeV and 20 MeV$\leqslant E_x^{\rm IVSM}\leqslant$50 MeV, respectively. Thus the total GT strength is insensitive to the details of the distribution of the IVSM strength.

In the following we use $S_{\beta^-}=28.0\pm1.6$ as the total GT β^- strength of ^{90}Nb up to 50 MeV excitation. However, it should be noted that the amplitude of the cross section is sensitive to the optical model parameters. Thus the amount subtracted as the contribution from the IVSM state is not well determined. It should be also emphasized that the present estimation of the contribution of the IVSM state is based on the assumption that the whole IVSM strength is located below 50 MeV excitation. Obviously the final resolution of the contribution of the IVSM strength to the $L=0$ strength must await future studies.

C. Ikeda's sum rule

The GT β^+ strength of ^{90}Y was derived from the results of MD analysis of the ^{90}Zr$(n,p)^{90}$Y reaction at 198 MeV by Raywood *et al.* [50]. Their best estimate of the total GT β^+ strength (S_{β^+}) is $S_{\beta^+}=1.0\pm0.3$. Condé *et al.* [48] also extracted the S_{β^+} value of ^{90}Y from the double differential cross sections of the ^{90}Zr$(n,p)^{90}$Y reaction at 98 MeV. The S_{β^+} value of 1.7 ± 0.2 was obtained in their analysis. The uncertainties of the S_{β^+} values given above do not include the uncertainty in the GT β^+ unit cross section ($\hat{\sigma}_{\beta^+}$). The uncertainties of $\hat{\sigma}_{\beta^+}$ are about 5 and 9 % in the cases of Raywood *et al.* [50] and Condé *et al.* [48], respectively. Therefore these two S_{β^+} values are consistent with each other by taking into account the uncertainties of $\hat{\sigma}_{\beta^+}$. Here we adopt the S_{β^+} value of 1.0 ± 0.3 by Raywood *et al.* since the ambiguity originating from the effect of distortion at $T_n=198$ MeV is smaller than that at $T_n=98$ MeV.

The S_{β^-} value up to 50 MeV excitation obtained in the present study is $S_{\beta^-}=28.0\pm1.6$. Therefore the total GT β^- strength minus the total GT β^+ strength becomes

$$S_{\beta^-}-S_{\beta^+}=(28.0\pm1.6)-(1.0\pm0.3)$$
$$=27.0\pm1.6. \quad (24)$$

This $S_{\beta^-}-S_{\beta^+}$ value is about (90 ± 5)% of Ikeda's sum rule value of $3(N-Z)=30$. The uncertainty of the $S_{\beta^-}-S_{\beta^+}$ value in Eq. (24) does not include the uncertainty coming from the uncertainty of the GT unit cross section. The uncertainties of S_{β^-} and S_{β^+} coming from the uncertainty of the GT unit cross section are 5.4 and 0.1, respectively. As a result the $S_{\beta^-}-S_{\beta^+}$ value has an uncertainty originating from the uncertainty of the GT unit cross section of 5.4. In the calculation of the $S_{\beta^-}-S_{\beta^+}$ value in Eq. (24), we used the S_{β^-} value up to 50 MeV excitation to avoid the systematic uncertainty of the B(GT) values coming from the ambiguity of the results in the MD analysis. However, the present MD analysis shows that there is a possibility of some GT strength existing beyond 50 MeV excitation, which means that the $S_{\beta}-S_{\beta^+}$ value of 27.0 can be assumed as a minimum value. Therefore the quenching of the GT strength due to the ΔN^{-1} admixture into the $1p1h$ GT state seems to be very small.

D. Model limitation

As a final remark we would like to mention some model limitations used in the MD analysis which may affect the $L=0$ strength extracted from the present data.

In the present DWIA calculations, the shallow binding energy is assumed to simulate the unbound single particle state. Although the similar assumption is frequently used for the analyses of high lying giant resonances, it is an open question as to how well the DWIA calculations based on this assumption are able to describe the experimental data, particularly if it is applied to the highly excited states such as 50 MeV. Therefore the theoretical work for the unbound single particle wave functions is needed to assess the size of the ambiguity arising from this approximation.

Recently it was reported by several authors [51–53] that the DWIA calculation has a difficulty in reproducing the experimental $L=1$ angular distribution at very forward angles where the $L=0$ transition, i.e., GT strength, is important. Based on the analysis for the ^{16}O$(p,n)^{16}$F$(2^-;0.4$ MeV) transition, Mercer *et al.* [53] have proposed deepening the reaction Q value, 8 MeV more negative than the proper Q value, in the DWIA calculation to get better agreement with data. Although there is no *a priori* reason for this and, moreover, such a difficulty is not known experimentally for the medium and heavy nuclei, we have examined the effect of this modification in the DWIA calculation according to their prescription. It is found that the effect is about -2.3 in B(GT) unit. This means a part of the GT strength is now reassigned as the 2^- strength and consequently the total S_{β^-} value decreases accordingly. Since this Q-value modification gives a moderate change in S_{β^-}, it is also important to study experimentally whether the similar difficulty of fitting exists or not in medium and heavy nuclei.

VI. CONCLUSIONS

In summary, we have measured the double differential cross sections at seven angles between 0.0° and 12.3° and

polarization transfer D_{NN} at 0° for the ^{90}Zr(p,n) reaction at an incident energy of 295 MeV. The MD technique is applied to the measured cross sections to extract the $L=0$ cross section. The present analysis assigns a considerable $L=0$ cross section above the GT giant resonance region up to 50 MeV excitation. The $L=0$ cross section deduced from the MD analysis has been extrapolated to $(q,\omega)=(0,0)$ to obtain the GT transition strength B(GT). Although the SRPA calculation by Drożdż *et al.* describes the distribution of the GT strength very well, the strength in the continuum is underestimated by about 0.2 MeV^{-1}. The second-order perturbative calculation by Bertsch and Hamamoto, on the contrary, agrees with the GT strength in the continuum. The obtained GT strength in the continuum region of excitation energies between 20 and 50 MeV is 0.45 MeV^{-1}, which agrees fairly well with the prediction of 0.48 MeV^{-1} of Bertsch and Hamamoto. The sum of B(GT) values up to 50 MeV excitation is $S_{\beta^-}=34.2\pm1.6$, which corresponds to about (114 ± 5)% of the minimum value of the GT sum rule.

We have also examined the possible contribution of the IVSM strength to the $L=0$ cross section obtained from the MD analysis. The DWIA calculation predicts $\sigma_{\mathrm{c.m.}}(0°)=9.9$ mb/sr for the IVSM state at 35 MeV excitation if the IVSM strength associated with $r^2[\sigma\otimes Y^{M=0}_{L=0}]_{J^\pi=1^+}\tau_-$ is fully exhausted. The total GT strength summed over the region up to 50 MeV excitation is $S_{\beta^-}=28.0\pm1.6$, or about (93 ± 5)% of the minimum value of the sum rule $3(N-Z)=30$, after subtracting the contribution of the IVSM strength to the $L=0$ cross section obtained from the MD analysis. It is also found that the total GT strength obtained after subtracting the contribution of the IVSM strength is insensitive to the details of the distribution of the IVSM strength. However, the amplitude of the cross section is sensitive to the optical model parameters. Therefore, the subtraction of the contribution from the IVSM state is ambiguous and further studies are needed to clarify the contribution of the IVSM strength.

The total GT β^- strength minus the total GT β^+ strength was calculated by using the present results and the S_{β^+} value reported by Raywood *et al.* [50]. The result is $S_{\beta^-}-S_{\beta^+}=27.0\pm1.6$ which corresponds to (90 ± 5)% of Ikeda's sum rule value of $3(N-Z)=30$. In the calculation of the $S_{\beta^-}-S_{\beta^+}$ value, we used the S_{β^-} value up to 50 MeV excitation to avoid the systematic uncertainty coming from the ambiguity of the results in the MD analysis. The present MD analysis, however, shows that there might be some GT strength beyond 50 MeV excitation. Thus the obtained $S_{\beta^-}-S_{\beta^+}$ value of 27.0 can be assumed as a minimum value. From this we conclude that the quenching of the GT strength due to the ΔN^{-1} admixture into the $1p1h$ GT state seems to be very small.

ACKNOWLEDGMENTS

We are extremely grateful to Y. Watanabe and M. Kawai for the SCDW calculation of the two-step contribution in the cross sections. We would like to thank K. Muto for the calculation of one-body transition amplitudes, and A. Okihana and N. Koori for their help in the early stages of the construction and development of the NPOL2 system. The experiment was performed at RCNP under Program No. E57. This work is supported in part by the Grants-in-Aid for Scientific Research Nos. 6342007 and 04402004 of the Ministry of Education, Science and Culture of Japan. One of the authors (T.W.) would like to also acknowledge the partial support by the Grant-in-Aid of the Japan Society for the Promotion of Science (JSPS) of Ministry of Education, Science and Culture of Japan.

[1] R. R. Doering, A. Galonsky, D. M. Patterson, and G. F. Bertsch, Phys. Rev. Lett. **35**, 1691 (1975).
[2] D. E. Bainum, J. Rapaport, C. D. Goodman, D. J. Horen, C. C. Foster, M. B. Greenfield, and C. A. Goulding, Phys. Rev. Lett. **30**, 1751 (1980).
[3] C. D. Goodman, C. A. Goulding, M. B. Greenfield, J. Rapaport, D. E. Bainum, C. C. Foster, W. G. Love, and F. Petrovich, Phys. Rev. Lett. **44**, 1755 (1980).
[4] D. J. Horen *et al.*, Phys. Lett. **95B**, 27 (1980).
[5] D. J. Horen *et al.*, Phys. Lett. **99B**, 383 (1981).
[6] C. Gaarde, J. Rapaport, T. N. Taddeucci, C. D. Goodman, C. C. Foster, D. E. Bainum, C. A. Goulding, M. B. Greenfield, D. J. Horen, and E. Sugarbaker, Nucl. Phys. **A369**, 258 (1981).
[7] K. Ikeda, S. Fujii, and J. I. Fujita, Phys. Rev. Lett. **3**, 271 (1963).
[8] C. Gaarde, J. S. Larsen, M. N. Harakeh, S. Y. van der Werf, M. Igarashi, and A. Müller-Arnke, Nucl. Phys. **A334**, 248 (1980).
[9] C. Gaarde, Nucl. Phys. **A369**, 127c (1983).
[10] M. Ericson, A. Figureau, and C. Thévenet, Phys. Lett. **45B**, 19 (1973).
[11] E. Oset and M. Rho, Phys. Rev. Lett. **42**, 47 (1979).
[12] I. S. Towner and F. C. Khanna, Phys. Rev. Lett. **42**, 51 (1979).
[13] K. Shimizu, M. Ichimura, and A. Arima, Nucl. Phys. **A226**, 282 (1974).
[14] A. Arima and H. Hyuga, in *Mesons in Nuclei*, edited by M. Rho and D. H. Wilkinson (North-Holland, Amsterdam, 1979), p. 683.
[15] G. F. Bertsch and I. Hamamoto, Phys. Rev. C **26**, 1323 (1982).
[16] T. N. Taddeucci, C. A. Goulding, T. A. Carey, R. C. Byrd, C. D. Goodman, C. Caarde, J. Larsen, D. Horen, J. Rapaport, and E. Sugarbaker, Nucl. Phys. **A469**, 125 (1987).
[17] M. A. Moinester, Can. J. Phys. **65**, 660 (1987).
[18] W. P. Alford *et al.*, Phys. Lett. B **179**, 20 (1986).
[19] R. D. Smith and J. Wambach, Phys. Rev. C **36**, 2704 (1987).
[20] Y. Watanabe and M. Kawai, Nucl. Phys. **A560**, 43 (1993).
[21] Y. Watanabe and M. Kawai (private communication).
[22] S. Drożdż, V. Klemt, J. Speth, and J. Wambach, Phys. Lett. **166B**, 18 (1986).
[23] H. Sakai, H. Okamura, H. Otsu, T. Wakasa, S. Ishida, N. Sakamoto, T. Uesaka, Y. Satou, S. Fujita, and K. Hatanaka, Nucl. Instrum. Methods Phys. Res. A **369**, 120 (1996).
[24] H. Sakai, H. Okamura, S. Ishida, K. Hatanaka, and T. Noro, Nucl. Instrum. Methods Phys. Res. A **320**, 479 (1992).

[25] T. N. Taddeucci *et al.*, Phys. Rev. C **41**, 2548 (1990).
[26] M. W. McNaughton *et al.*, Phys. Rev. C **45**, 2564 (1992).
[27] D. V. Bugg and C. Wilkin, Nucl. Phys. **A467**, 575 (1987).
[28] G. G. Ohlsen, Rep. Prog. Phys. **35**, 717 (1972).
[29] H. Sakai *et al.*, Phys. Rev. C **35**, 344 (1987).
[30] T. Wakasa *et al.* (in preparation).
[31] D. J. Mercer, Ph.D. Thesis, University of Colorado, 1992.
[32] T. N. Taddeucci *et al.*, Phys. Rev. C **33**, 746 (1986).
[33] A. K. Kerman, H. McManus, and R. M. Thaler, Ann. Phys. (N.Y.) **8**, 551 (1959).
[34] W. G. Love and M. A. Franey, Phys. Rev. C **24**, 1073 (1981).
[35] J. M. Moss, Phys. Rev. C **26**, 727 (1982).
[36] T. Wakasa *et al.*, Phys. Rev. C **51**, R2871 (1995).
[37] R. Schaeffer and J. Raynal, Program DWBA70 (unpublished); J. Raynal, Nucl. Phys. **A97**, 572 (1967); J. R. Comfort, Extended version DW81 (unpublished).
[38] S. K. Nanda, Ph.D. Thesis, The State University of New Jersey, 1985.
[39] S. Qing-biao, F. Da-chun, and Z. Yi-zhong, Phys. Rev. C **43**, 2773 (1991).
[40] K. Muto, H. Yamazaki, T. Oda, and H. Horie, Phys. Lett. **165B**, 25 (1985); T. Muto (private communication).
[41] M. A. Franey and W. G. Love, Phys. Rev. C **31**, 488 (1985).
[42] J. Kasagi, G. M. Crawley, E. Kashy, J. Duffy, S. Gales, E. Gerlic, and D. Friesel, Phys. Rev. C **28**, 1065 (1983).
[43] J. L. Horton, C. L. Hollas, P. J. Riley, S. A. A. Zaidi, C. M. Jones, and J. L. C. Ford, Jr., Nucl. Phys. **A190**, 362 (1972).
[44] T. N. Taddeucci, Can. J. Phys. **65**, 557 (1987).
[45] T. Wakasa *et al.*, Nucl. Phys. **A599**, 217c (1996).
[46] N. Auerbach, J. D. Bowman, M. A. Franey, and W. G. Love, Phys. Rev. C **28**, 280 (1983).
[47] N. Auerbach and A. Klein, Phys. Rev. C **30**, 1032 (1984).
[48] H. Condé *et al.*, Nucl. Phys. **A545**, 785 (1992).
[49] A. Bohr and B. R. Mottelson, *Nuclear Structure* (Benjamin, New York, 1969), Vol. 2, p. 341.
[50] K. J. Raywood *et al.*, Phys. Rev. C **41**, 2836 (1990).
[51] A. Celler *et al.*, Phys. Rev. C **43**, 639 (1991).
[52] K. H. Hicks, A. Celler, O. Häusser, R. Henderson, K. P. Jackson, B. Pointon, J. Rapaport, M. Vetterli, and S. Yen, Phys. Rev. C **43**, 2554 (1991).
[53] D. J. Mercer *et al.*, Phys. Rev. C **49**, 3104 (1994).